Volume 5, Issue 1, 2016, 346-353 ISSN 2284-6808

Letters in Applied NanoBioScience

www.NanoBioLetters.com

Original Research Article Open Access Journal

Received: 22.08.2015 / Revised: 20.11.2015 / Accepted: 15.12.2015 / Published on-line: 01.01.2016

# CNT-enhanced Raman spectroscopy and its application: DNA detection and cell visualization

**Alexander Sergeevich Egorov [1], Valentina Petrovna Egorova [2], Halina Vladislavovna Grushevskaya [3,*], Nina Georgievna Krylova [3], Igor Vladimirovich Lipnevich [3], Taisija Ivanovna Orekhovskaya [4], Boris Georgievich Shulitsky [4]**

[1]Institute of Physiology, Nat. Acad. Sci. of Belarus, Belarus
[2]Belarusian State Pedagogical University,Belarus
[3]Belarusian State University, Belarus
[4]Belarusian State University of Informatics and Radioelectronics, Belarus

*corresponding author e-mail address: ***grushevskaja@bsu.by***

## ABSTRACT

We have experimentally observed an enhancement of Raman scattering on surface plasmons in Si coated by complexes of ds-DNA with carbon nanotubes (CNTs) chemically modified and functionalized by stearic acid. This enhancement is due to appearance of free charge carriers in CNTs at the complexification. We found out that similar surface-enhanced Raman scattering phenomenon takes place in a propidium iodide monomolecular layer on CNT-bundle arrays which are deposited on nanoporous anodic alumina coated by ultrathin metal-containing conducting Langmuir-Blodgett film. A method of two-dimensional systems visualization based on the CNT-enhanced Raman spectroscopy has been proposed. This method has been applied for visualization of focal adhesion sites on cellular membranes.

**Keywords:** *Raman spectroscopy, SERS, dye-labelled DNA, cell visualization.*

## 1. INTRODUCTION

Surface enhanced Raman spectroscopy (SERS) is a promising method with improved sensitivity which allows to detect DNA sequence hybridization [1, 2], structural and functional properties of nanoscale membrane structures of living cells and antigens in a data-rich manner [3]. Usage of surface enhanced resonance Raman scattering allows to obtain Raman spectra of such nanostructures as monomolecular Langmuir-Blodgett (LB) films deposited on a surface with silver islands [4]. Bilayer phospholipid cellular membranes are similar in structure to LB-films. In papers [5, 6], the surface enhanced Raman spectroscopy has been proposed to study cells and subcellular structures on a monolayer of gold or silver nanoparticles coated by surfactant. However, the usage of metal surface limits SERS applicability in biotechnology [3]. Surface-modified gold or silver nanoparticles are accumulated inside cells or selectively bind with membrane receptors, disrupting cell functioning. Another problem of the method is the reproducible preparation of high-sensitive SERS-active nanostructures with narrow distribution in enhancement factor values [7]. Size of gold or silver nanoparticles (more than 20 nm) is large comparing with a size of a single cellular focal adhesion site (about 10 nm). [8]. The focal contact is terminated by binding of integrin receptor with hydrophobic sites of extracellular matrix (ECM), for example, culturing substrate. Integrin receptor portions protruding to the intermembrane space and interacting with ECM play a role of cellular supporting structure. The height of this external part is about 10–15 nm [9]. Because of this, the resolution of known methods which use metal nanoparticles is not sufficient to visualize distribution of cellular supporting structures (focal adhesion sites). This explains a large spread of experimental data of focal adhesion site sizes: the width is about 1–3 μm and the length is about 2–10 μm [9, 10].The use of carbon nanotubes in SERS is hampered due to the lack of free charge carriers at the Fermi level in graphene and graphene-like materials[11-14].

In this paper we show that dye-labelled double-stranded (ds) DNA fluorescence quenching at ds-DNA wrapping around CNTs is due to a charge and energy transfer to carbon nanotubes with a small number of walls (mCNTs). This transfer leads to transport of free charge carriers in mCNTs. The resonance of plasmon oscillations in CNT at eigen frequencies of silicon surface vibrations gives rise to the phenomenon of CNTs-enhanced Raman scattering in Si. We found out that similar charge and energy transfer on mCNT takes place on a surface of nanoporous anodic alumina (AOA) coated by ultrathin conducting metal-containing LB-film of thiophene-pyrrole oligomers. The phenomenon of mCNT-enhanced Raman scattering is also observed for a monomolecular layer (monolayer) of fluorophore (propidium iodide (PI)) on a LB-mCNT-bundle arrays deposited on AOA with the LB-film. mCNT-enhanced Raman scattering in PI monolayer has been used for visualization of nanostructures of focal adhesion type on the outer side of membrane of living C6 rat glioma cells. The goal of the paper is to reveal and explain the phenomenon of mCNT-enhanced resonance Raman scattering and to apply this phenomenon for visualization of cell-matrix adhesion sites of C6 cells stained with propidium iodide. The paper is organized as follows. In Section 2 the methods of investigation are described. In Section 3 we establish the appearance of free charge carriers in mCNT at complexification of mCNT with ds-DNA that

leads to intensity increase of Raman scattering on surface plasmons in Si coated by mCNT/ds-DNA-complex monolayer. Further in the section we represent the method of two-dimensional (2d) systems visualization. This method is based on the enhancement of Raman scattering in PI monolayer on a surface of a LB-mCNT-cluster deposited on AOA with the LB-film. And at last the proposed method is used to visualize focal adhesion sites on cellular membranes. In Conclusions we summarize our findings.

## 2. EXPERIMENTAL SECTION

### 2.1. Materials.

RNA and proteins fractions in high-purity double-strand DNA (1.03 mg/ml in $10^{-5}$ M $Na_2CO_3$ buffer medium) were less that 0.1% (optical density ratio $D_{160}/D_{230}$ = 2.378 and $D_{160}/D_{280}$ = 1.866, respectively). mCNT with diameters ranging from 2.0 to 10 nm and a length of 2.5 μm were obtained by the method of chemical vapor deposition (CVD-method) [15]. mCNT were covalently modified by carboxyl groups and non-covalently functionalized by stearic acid molecules [16]. Complexes ds-DNA/mCNT were obtained by means of ultrasonic treatment of alcoholic solution of ds-DNA with mCNT [17]. The complexes ds-DNA/mCNT were mixed with a solution of stearic acid in deionized water or in hexane. The resulting mixtures were homogenized by ultrasonic treatment to form hydrophilic or hydrophobic (reverse) micelles of stearic acid with ds-DNA/mCNT complexes inside them [18]. C6 rat glioma cells obtained from culture collection of Institute of Epidemiology and Microbiology (Minsk) were grown on aligned mCNT arrays in a Dulbecco's modified Eagle medium (DMEM) (Sigma, USA) supplemented with 10 % fetal bovine serum and $1 \cdot 10^{-4}$ g/ml gentamycin at 37 °C in a humidified 5 % $CO_2$ atmosphere. Propidium iodide (Sigma, USA), luminescence of which is high-intensive in hydrophobic environment, for example, when it intercalates into DNA sequence, but is low-intensive in hydrophilic medium (because of quenching by water molecules), has been used as a fluorescent probe [19].

Fabrication of AOA films (thickness of 200–300 nm) on optical glass and fabrication of AOA membranes (thickness of 20.0 μm) were carried out by means of two-phasic anodic treatment in 10 % sulfuric acid solution at voltage of 10 V and temperature of 2ºC [20]. The diameter of AOA pore was equal to 10 nm.

Langmuir monolayers from 3-hexadecyl-2,5-di (thiophen-2-yl)-1*H*-pyrrole (thiophene-pyrrole) with chemically bounded hydrophobic 16-link hydrocarbon chain and LB-monolayers from carboxylated mCNT functionalized by stearic acid were prepared on an automated home-built Langmuir trough with controlled deposition on a substrate [21]. Aqueous solution of ferric nitrate $Fe(NO_3)_3$ or ferric chloride $FeCl_3$ with or without $Ce_2(SO_4)_3$ with pH=1.65 adjusted by addition of hydrochloric acid HCl was used as a subphase for thiophene-pyrrole monolayer formation. All salt solutions have been prepared with deionized water with resistivity 18.2 MΩ cm. Deionized water was used as a subphase for mCNT-monolayer formation. All other reagents were of analytical grade.

### 2.2.Methods.

Microdiffraction patterns and electron microscopic images were obtained by means of transmission electron microscope JEM-100CX (JEOL, Japan) (TEM) at accelerating voltage of 100 kV. Structural analysis has been performed on the objects previously deposited on a copper grid with a formvar polymer coating or on AOA membranes that were made very thin by etching. Spectral studies in ultraviolet and visible ranges were carried out using a confocal micro-Raman spectrometer Nanofinder HE («LOTIS-TII», Tokyo, Japan–Belarus) with laser excitation at wavelengths 473 nm or 532 nm and with a spectrofluorimeter CM2203(Solar, Belarus).

## 3. RESULTS SECTION

### 3.1.Surface enhanced Raman scattering in stearic acid micelles and DNA/mCNT complexes on Si surface.

#### 3.1.1. Structural analysis of DNA/mCNT complexes.

TEM-images of carboxylated mCNTs are shown in fig.1a. mCNTs have an "open"-type ends. DNA/mCNT complexes an electron-dense nucleotide layer self-organized on mCNT surface [22-24]. As shown in fig. 1b, practically black nucleotide shell links ("glues") the dazzling white carbon nanotubes one to another, that creates conditions for charge transport and energy transfer. The sites in which ds-DNA glues one mCNT to another two mCNTs are pointed out by arrows in fig. 1b.The hydrophobic reverse micelles from stearic acid with mCNTs and/or ds-DNA do not spread on hydrophilic Si and AOA surfaces, but shape space-saving (see fig. 1c).

#### 3.1.2. Raman spectroscopy of mCNT.

Low-intensive Raman spectra of dried mCNT without non-covalent functionalization by stearic acid are shown in fig. 2. Raman spectra of graphene and graphen-like materials have been studied in detail (see [25] and its references). The spectral bands *D* and $D'$ in fig. 2 reveal the existence of defects in graphene lattice and correspond to optical transverse and longitudinal in-plane vibrations in the vicinity of K point of the Brillouin zone. These phonons are nucleus oscillations in the field (term) of $\pi(p_z)$-electrons in valence band or $\pi^*$(d)-electrons in conduction band.

The peak $D''$ is a longitudinal acoustic mode in the vicinity of K point. The spectral band *G* originates also from in-plane carbon atoms vibrations, but in the electronic-vibrational term of $sp^2$–hybridized electrons. This resonance corresponds to optical surface phonons in the vicinity of Γ point of the Brillouin zone. $D^3$ and $D^4$ are transverse and longitudinal acoustic branches of in-plane vibrations in the vicinity of Γ point. 2*D* is a peak of two-phonon absorption (doubled *D* mode). Radial Breathing Mode (RBM) for mCNT is observed in frequency range from 60 to 430 $cm^{-1}$, as shown in fig. 2. Diameters of mCNTs can be estimated by RBM mode [26,27]. Calculations by RBM mode give the diameters of 2 nm and less for mCNT presented in our sample.

**3.1.3. Raman spectroscopy of ds-DNA.** Raman spectrum of ds-DNA-contained micelles which were dropped on a polished silicon support has all characteristic lines of Raman scattering on DNA, as shown in fig.3a.

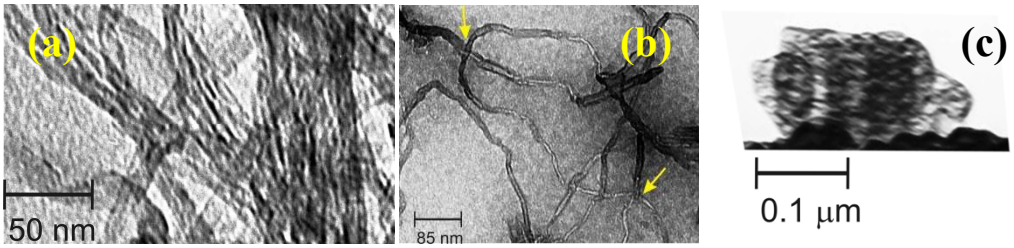


**Figure 1.** TEM-images of carboxylated mCNT 2d-bundle (a) and ds-DNA/mCNT complexes (b) on formvar coating; TEM-images of reverse micelle of stearic acid with mCNT on etched AOA membrane (c).

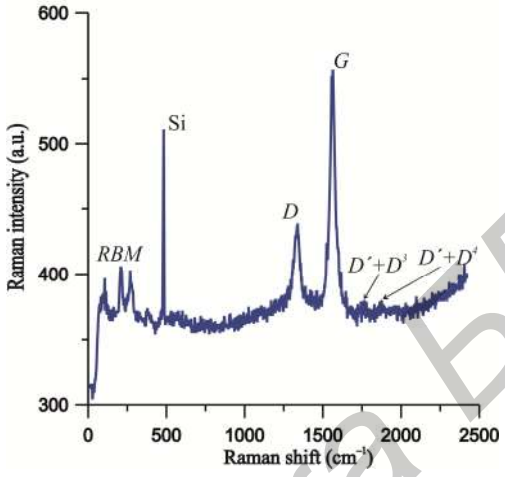


**Figure 2.** Raman spectrum of dried carboxylated mCNT when exited by green laser (532 nm) with power 20 mW.

**3.1.4. Raman spectroscopy of micelles with ds-DNA/mCNT complexes.**

The hydrophilic micelles spread on Si surface to 2d-monolayer. Fig. 4a shows Raman spectrum of 2d-monolayer of ds-DNA/mCNT complexes. One can see that the intensities of peaks corresponding to silicon vibrational mode and Si support laser plasmon peak frequency (fig. 3a) increase in the presence of ds-DNA/mCNT complexes on the surface (fig.4a). In contrast to ds-DNA/mCNT complexes in 2d-monolayer of spread hydrophilic micelles, ds-DNA/mCNT complexes in hydrophobic micelles have three-dimensional (3d) packaging. Raman spectra of ds-DNA/mCNT complexes inside hydrophobic micelles of stearic acid are shown in fig. 4b. The comparison fig.2 with fig. 4b indicates that the complexation significantly intensifies mCNT modes: $D$, $G$, $D'' + D$, $2D$, $D' + D$. The characteristic modes of ds-DNA in spectra in fig. 4 are not observed and, consequently, the quenching of DNA Raman bands occurs. This is due to transfer of electric charge carriers and quasi-particle excitation energy from nucleotide bases to mCNTs, that leads to excitation of surface plasmonic oscillations of Si support. The probability of electron transfer from valence $\pi(p_z)$- orbital of nucleotides to $\pi^*$(d)-orbital of mCNT is so high that DNA molecules Raman spectrum is quenched completely.

**3.1.5. Surface enhanced Raman scattering in ds-DNA/mCNT complexes monolayer on Si surface model.**

CNT is a graphene-like material. CNTs, similarly to graphene, possess high electroconductivity [11]. The charge carriers in graphene are negatively and positively charged quasi-particle excitations. Electrons and holes in undoped (pure) graphene are localized in separate region (so called "puddles") of cone valence zone [11] and do not appear in K point – the top of the Dirac cone. Although pure graphene has free charge carriers, because of graphene bipolarity, its Fermi level lies in K point where charge carriers are absent. Further we show that the additional electron density transferred from aromatic compounds can provide the Fermi level shift to graphene conductivity band.

At low intensities of electro-magnetic field $H_{ext}$ (laser excitation) the quantity of charge carried from DNA to CNT is negligible. Because of this, all additional electron density annihilates and released energy is spent on transfer of graphene charge carriers from valence band to conductivity one. Due to the fact that in a wide exciton spectrum of CNT there exist frequencies that coincide with plasma oscillation frequencies, Si plasmons parametrically resonate at these frequencies. This resonances wings the electron subsystem of Si and the intensities of Si Raman lines increase, as it follows from comparison of lower blue curves in fig. 4a and fig.3b.

At intermediate intensities of electro-magnetic field $H_{ext}$, due to a small number of localized charge carriers in pure graphene, not all additional electron density carried from aromatic compounds annihilates and a part of them becomes an impurity. Because of the fact that additional electrons on $\pi^*$-orbital of CNT are the localized d-electrons, one can consider this impurity as bubbles with localized d-electrons. The states of bubbles are stabilized by hole transfer from excitons and the decay of the last.

Such bubble of electron density with hole inside is similarly to an atom. Multi-photon absorption being due to the reflective diffraction on the boundary of the electron density bubble with a hole leads to mixing of d- and s-like orbitals.This mixed electron state of bubble is described by a wave function

$$|\Psi\rangle = |\mathrm{d}\rangle + f(H_{ext})|\mathrm{s}\rangle. \quad (1)$$

Let us consider the transition from p-orbital into the state (1) with full momentum $\vec{J} = \vec{j}_d + \vec{j}_s = \vec{L} + \vec{S}$; $J = 1$ at non-equilibrium spin $S = 0$ and angular momentum $L = 1$. The Hanle effect leads to splitting of the p-orbital. The transition from the state with momentum $J = 2(l–s) = 1$ with $l=1$ and $s=1/2$ is forbidden. This forbidden transition appears in Raman spectrum in fig. 4a as a small peak at frequency about 1410 $cm^{-1}$ (green intermediate curve) in addition to spectrum of CNT-enhanced Raman scattering on Si.

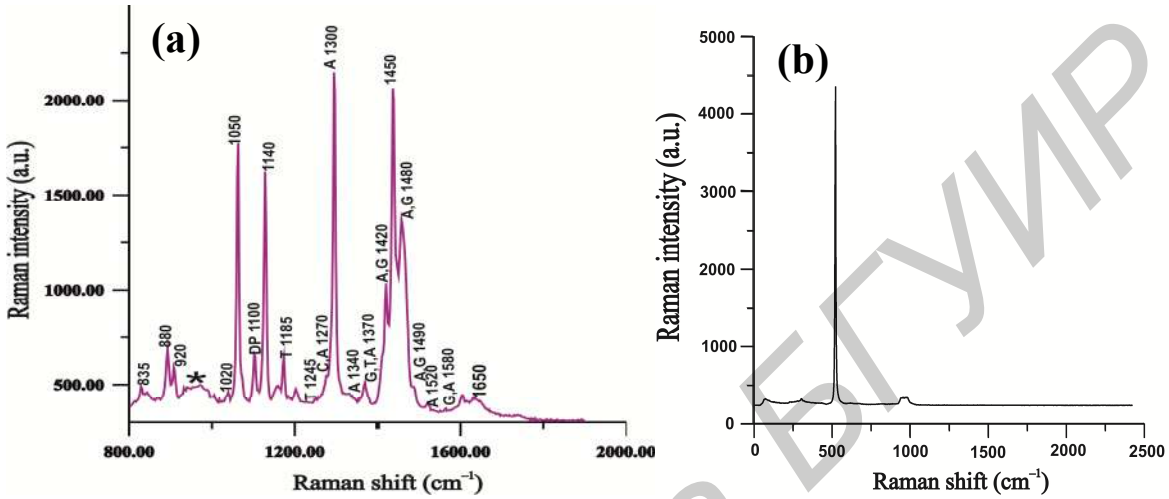


**Figure 3.** Raman spectrum of micelles formed in hexane solution of mixture from stearic acid with ds-DNA and dropped on Si (a); and Raman scattering on silicon support (b). The numbers indicate the characteristic frequencies of DNA vibrations; adenine, guanine, thymine and cytosine are designated by A, G, T and C, respectively; DP denotes phosphodiester bond. «*» indicates the laser peak of surface plasmons in Si. Laser power was 20 mW, exitation wavelength was 532 nm.

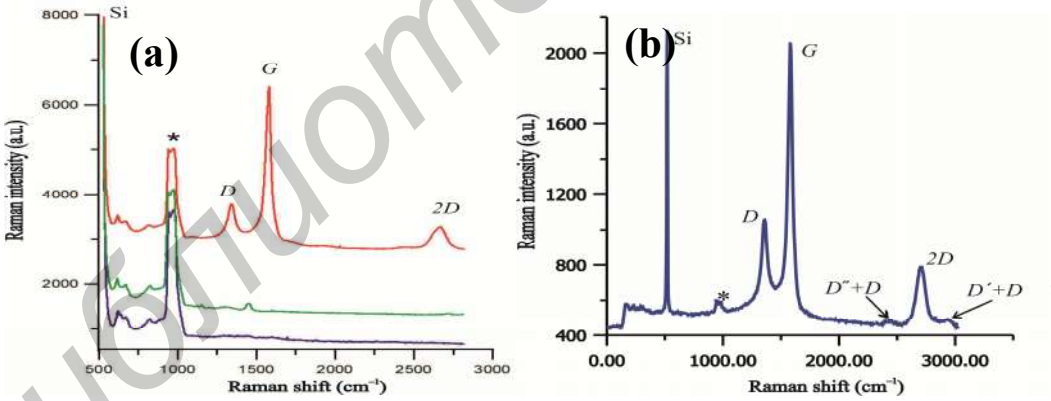


**Figure 4.** Raman spectra of stearic acid micelles with inside DNA/mCNT complexes on Si surface: (a) hydrophilic micelles; excitation by green laser (532 nm) with power 3.0, 5.76 and 20 mW for the low blue, intermediate green and top red curves, respectively; (b) hydrophobic micelles; excitation by blue laser (473 nm) with power 5.76 mW. Symbols «Si» and «*» designate vibrational mode of Si and the laser peak of plasma scattering in silicon, respectively.

At large intensities of laser excitation, the oscillatory Hanle effect that leads to degeneration of bubble p-like orbital is observed [29]. In this case, the atom-like bubbles consisted of d-electrons with holes as a donor impurity in the electron density canal so add missing electron density in the vicinity of K point via the resonant excitation of coherent negatively charged excitons $X^-$ in following way. Because of p-electrons transitions from degenerated p-orbitals with $S = 0$, $L = 0$ into the mixed state $S = 0$, $L = 1$ is allowed, the excited p-electrons can resonate with π*(d)-orbitals of CNT. The appearance of hybridization gap leads to transition of electrons on $\pi(p_z)$-orbitals of atoms C with emission of photons, energy of which is spent on the transition of graphene charge carriers (negatively charged excitons $X^-$) from valence band to the conductivity one. As a result, similarly to the case of low intensities of $H_{ext}$, the parametric resonance of Si vibrational and plasmon frequencies on eigen frequencies of free charge

carriers in CNT results in CNT-enhanced resonance Raman spectrum of Si shown in fig 4a, red curve. The donor impurity levels of bubbles with d-electrons appear in the process of hybridization of mixed state orbitals ($S$ = 0, $L$ = 1) with π*(d)-orbitals of CNT in conductivity band (K point of Brillouin zone) through the scattering of mixed state on the vibrational $D$- and $2D$-modes of CNT graphene-like band structure, as shown in fig. 4a, red curve. In addition, the quasi-particle excitations $X^-$ resonate with s-electrons of carbon atoms involved in $sp^2$-hybridization and, respectively, exciton energy is scattered in Raman band $G$, as represented in fig. 4a, red curve.

Let us calculate the exciton radius using the formula $r_{X^-} = \sqrt{\pi a d_c}/2$ [30]. Here $d_c$ is a thickness of the conducting part of a sample, in our case, the mCNT diameter, $a$ is an exciton radius in a bulk sample. For monolayer of ds-DNA/mCNT mixture the value of $a$ is equal to the size of ds-DNA/mCNT complex: from 10 to 20 nm; for micelles we choose $a$ being equal to their size (1 μm). Then, the calculated radius of exciton $X^-$ in micelles is appeared to be 10 times larger than in the monolayer.

Because of this, the weak coupling of electron-hole pairs in 3D-samples stipulates their localization on defects. As one can see from the comparison of fig. 4b and fig. 4a, at decrease of a number of free charge carriers, the number of pulses in parametric resonance reduces and, respectively, both intensity of laser plasma peak of Si Raman spectra and intensity of $X^-$-enhanced Raman spectral bands of graphene ($D$, $G$, $2D$) decrease. The localized excitons decay into $D+D'$ - and $D+D''$ -modes as shown in fig. 4b.

### 3.2. mCNT-enhanced resonance Raman spectroscopy with iodide propidium.

To hydrophobizate the hydrophilic surface of AOA (shown in fig. 5a), five metal-contained thiophene-pyrrole LB-monolayer in the high-ordered solid state were deposited on AOA [21]. The confocal image of this metal-containing thiophene-pyrrole LB-film is shown in fig. 5b. After that, two monolayers of functionalized mCNT were deposited on thiophene-pyrrole LB-film on AOA. The morphology of mCNTLB monolayers is shown in fig. 5c. As one can see in fig. 5c, the high-ordered LB-mCNT-clusters are 2d horizontally-aligned arrays, ends of which are vertically anchored on the surface of conducting thiophene-pyrrole LB-film. The diffraction pattern of LB-mCNT-clusters on the surface of thiophene-pyrrole LB-film is characterized by Kikuchi lines [17]. This means that deposited on thiophene-pyrrole LB-film LB-clusters of carboxylated non-covalently functionalized by stearic acid mCNT are crystallites. In the sites of contacts of vertical-aligned ends of mCNT-bundles with metal-containing LB-film, charge and energy transfer on LB-mCNT-clusters occurs.

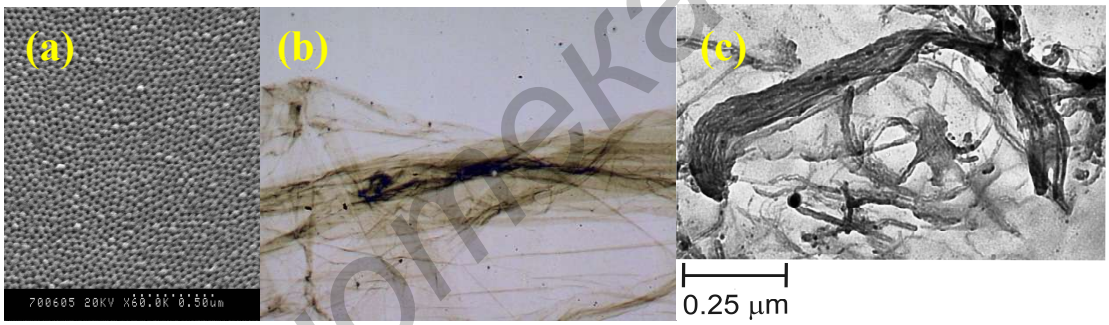


**Figure 5.** (a) The scanning electron microscopy image of AOA surface. (b) The confocal microscope image of metal-containing thiophene-pyrrole LB-film on Si. (c) TEM-image of mCNT-LB-cluster on support from the metal- containing thiophene-pyrrole LB-film on a formvar coating.

Raman scattering by fluorescent probe PI is resonant. Propidium iodide, according to fig. 6a, fluoresces in a wide range of wavelengths from 585 to 685 nm at excitation by green laser (532 nm). Raman spectra of PI aqueous solution on glass and LB-film are shown in fig. 6b. The Raman spectrum of PI on LB-mCNT-coating has two differences comparing with Raman spectrum of PI on a glass. First, the spectrum of PI on LB-mCNT-coatings has the maximum at frequency 1600 $cm^{-1}$, where PI on a glass practically does not fluoresce. Second, spectrum of PI on a glass has a shoulder at frequency 3600 $cm^{-1}$, where emission of PI on LB-mCNT-coating is practically absent. Because of the maximum of Raman spectrum of PI on LB-mCNT-coating coincides with G-mode of mCNT, the parametric resonance with the eigen frequencies of exciton free charge carriers, the existence of which has been discussed earlier, results in the enhancement of Raman scattering by PI. The resonance Raman scattering scanning of LB-mCNT-layer surface has been carried out. As shown in fig. 7, the maximal mCNT enhancement of PI fluorescence takes place in a fold of LB-mCNT-film at frequency 1600 $cm^{-1}$. And, vice versa, the quenching of PI fluorescence occurs outside of the LB-mCNT-film fold at frequency 3600 $cm^{-1}$. As it has been noticed previously, PI molecules fluorescence is quenched by water molecules. Then the maximal intensity of fluorescent probe emission takes place in the hydrophobic fold of LB-mCNT-film. These peculiarities of the confocal images of PI distribution on LB-mCNT-coating will be used further for the analysis of structural organization of C6 rat glioma cell monolayer.

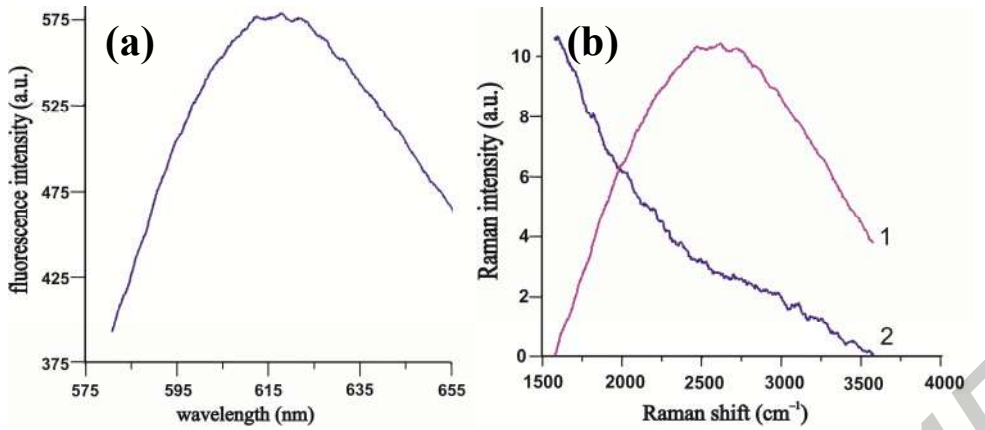


**Figure 6.** Spectra of PI fluorescence (a) and PI Raman scattering on glass and LB-mCNT-coating, curve 1 and 2 in fig. 6b, respectively.Excitation by green laser (532 nm) with power 0.06 mW.

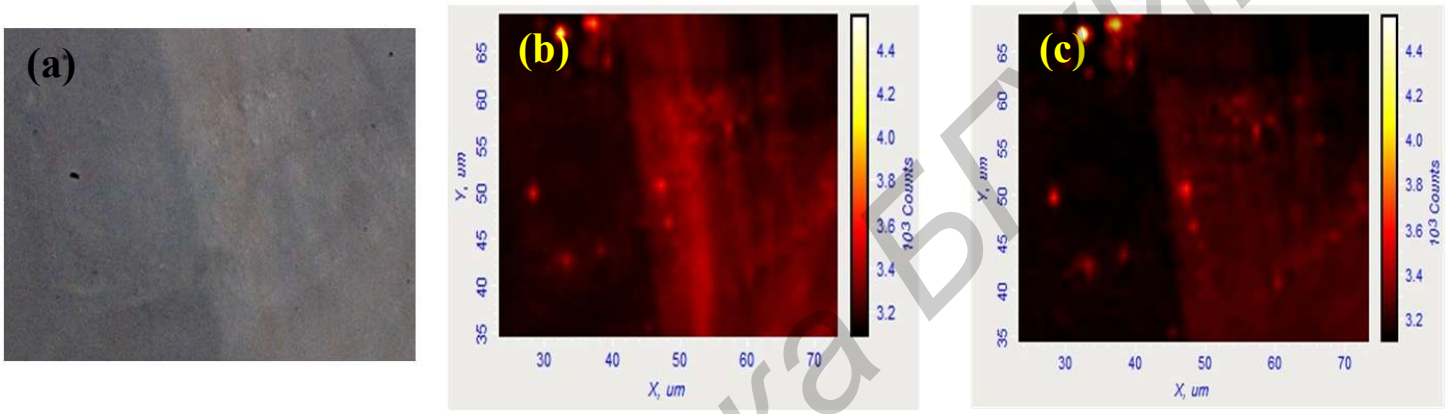


**Figure 7.** Confocal microscope images of mCNT-contained LB-coating in fold of which the PI molecules intercalate. Excitation by green laser (532 nm), the distribution of Raman scattering intensity at Raman shift: 1600 $cm^{-1}$ (b) and 3600 $cm^{-1}$ (c).

### 3.3. Visualization of cellular monolayer.

To visualize the structure of C6 cell monolayer grown on the studied LB-coating, cells were stained with propidium iodide. The resonance Raman scattering scanning of C6 cell monolayer has been carried out at two frequencies: 1600 and 3600 $cm^{-1}$.

In fig. 8 the typical images of PI distribution in cells grown on a cover glass (fig. 8a–f) and LB-films (fig. 8g–i) are shown. In control living cell monolayer on glass (positive control), PI practically does not penetrate into nuclei, the probe forms rare low-fluorescent complexes with nucleotides in cytoplasm, as shown in figs. 8b and 8c.If cell membrane structures are destroyed, the fluorescent probe molecules intercalates in nucleotide strand losing its hydrate shell. In the absence of fluorescence quenching by water molecules, the PI fluorescence increases more than 2 times (figs. 8e and 8f). Without mCNT in LB-film the enhanced Raman scattering of PI molecules does not occur and, respectively, the confocal fluorescent images of living and died cells on glass are brighter at Raman shift 3600 $cm^{-1}$ than at 1600 $cm^{-1}$. As shown in fig 8i, resonance Raman scattering of PI at 3600 $cm^{-1}$ is practically absent that indicates the viability and wholeness of cells grown on LB-coating. The well-defined fluorescent image of cells with dark nuclei and bright points of high-intensive luminescence are registered when resonance Raman scattering of PI at 1600 $cm^{-1}$ is detected (fig. 8h). The domains of high-intensive luminescence have a diameter about 1 μm and placed along periphery of cells (for all cells in scanning zone) and partially around cellular nucleus (for lower cell in scanning zone). The distribution and sizes of found domains correspond to the focal adhesion sites of cells.

One can see in fig. 8g that the upper cell is a spread cell with well-defined outlined nucleus that indicates cellular state as interphase or quiescence G0. The focus of confocal microscope lies approximately in the center of the cell. Because of this, the visible sites of focal adhesions are placed near periphery. The body of the lower cell is more round and focusing plane is closer to a lower wall of the cell, so the cellular nucleus in fig. 8g is of bad view and visible "horizontal slice" of nucleus is smaller in size in comparison with the upper cell.Because of this, the focal contacts attaching a lower cell to substrate not only on periphery but under cellular body are visualized.

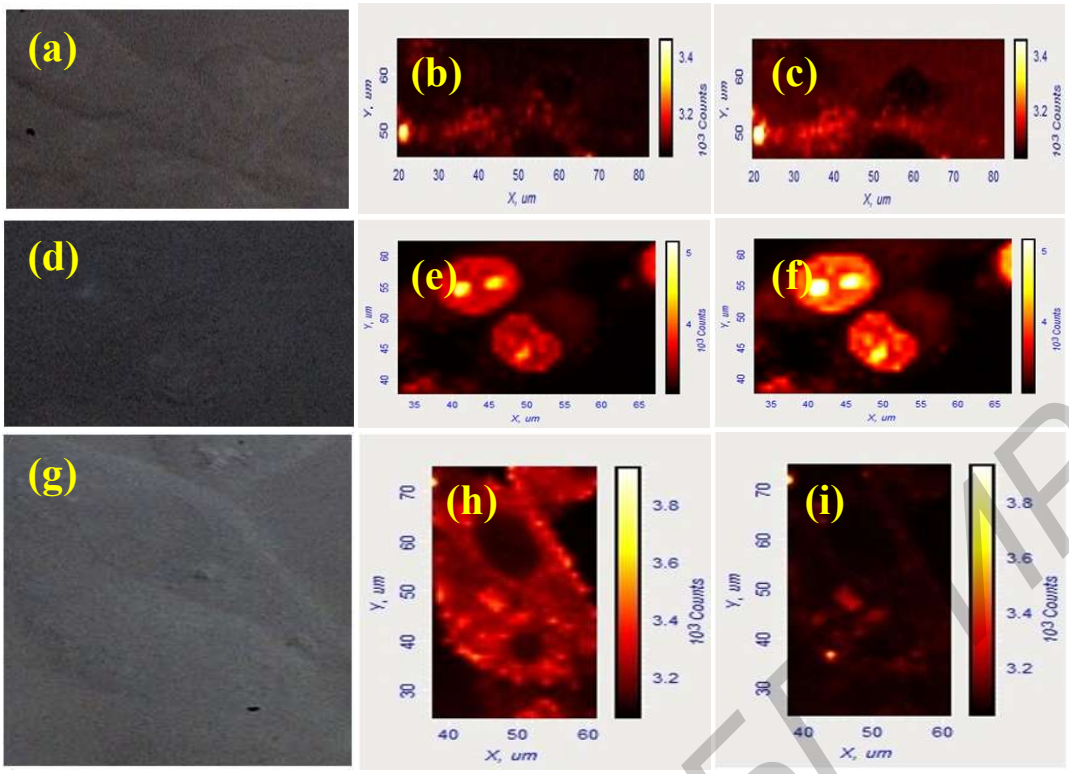


**Figure 8.** Confocal microscope images of C6 rat glioma cells grown on glass (positive control, 4 cells) for 72 h (a–c) and after 0,01 % TritonX-100 treatment (negative control, 2 cells) (d–f), on LB-coating with mCNT (g–i, 2 cells). Cells were stained with propidium iodide for 5 min. Excitation by green laser (532 nm), emission detection at frequencies (Raman shifts): 1600 $cm^{-1}$ (in centre) and 3600 $cm^{-1}$ (right).

## 4. CONCLUSIONS

To summarize, the existence of charge transfer from ds-DNA to carbon nanotubes with a small number of walls has been found out. This charge transfer results in the appearance of free charge carriers transport in mCNT. The high-conducting mCNTs in LB-coating enhances the resonance Raman scattering on both silicon surface modes and propidium iodide fluorescent probe monolayer. The last phenomenon allows to visualize nanostructured surface of living cells grown on biocompatible coating such as thin metal- and mCNT-contained LB-film on nanoporous anodic alumina. It has been established that the diameter of focal adhesion sites is about 1 μm. The set of the integrin receptor zones is high-ordered and periodical one.

## 5. REFERENCES

[1] K. S. McKeating, J. A. Dougan, K. Faulds, Nanoparticle assembly for sensitive DNA detection using SERRS, *Biochem. Soc. Trans.,* 40, 597-602, **2012**.
[2] J. Bansal, I. Singh, P. K. Bhatnagar, P. C. Mathur. DNA sequence detection based on Raman spectroscopy using single walled carbon nanotube, *J. Biosci. Bioengin.*, 115, 4, 438-441, **2013**.
[3] D. Graham, K. Faulds, D. Thompson, F McKenzie, R. Stokes, C. Dalton, R. Stevenson, J. Alexander, P. Garside, E. McFarlane, Functionalized nanoparticles for bioanalysis by SERRS, *Biochem. Soc. Trans.*, 37, 697-701, **2009**.
[4] C. Constantino, J. Duff, R. Aroca, Surface enhanced resonance Raman scattering imaging of Langmuir–Blodgett monolayers of bis (benzimidazo) thioperylene, *SpectrochimicaActa Part A.*, 57, 1249-1259, **2001**.
[5] R. R. Sathuluri, H. Yoshikawa, E. Shimizu, M. Saito, E. Tamiya, Gold nanoparticle-based surface-enhanced Raman scattering for noninvasive molecular probing of embryonic stem cell differentiation, *PLoS ONE*, 6, 8, e22802, **2011**.
[6] C. M. MacLaughlin, N. Mullaithilaga, G. Yang, S. Y. Ip, C. Wang, G. C. Walker, Surface-enhanced Raman scattering dye-labeled Au nanoparticles for triplexed detection of leukemia and lymphoma cells and SERS flow cytometry, *Langmuir*, 29, 1908-1919, **2013**.
[7] Y. Fang, N.-H.Seong, D. D. Dlott, Measurement of the distribution of site enhancements in surface-enhanced Raman scattering, *Science*, 321, 388-392, **2008**.
[8] K.-F. Giebel, C. Bechinger, S. Herminghaus, M. Riedel,P. Leiderer, U. Weiland, M. Bastmeyer, Imaging of cell/substrate contacts of living cells with surface plasmon resonance microscopy, *Biophys. J.*, 76, 509-516, **1999**.
[9] V. Petit, J.-P. Thiery, Focal adhesions: structure and dynamics, *Biology of the Cell.,* 92, 477-494, **2000**.
[10] A.W. Peterson, M. Halter, A. Tona, K. Bhadriraju, A. L. Plant, Surface plasmon resonance imaging of cells and surface-associated fibronectin, *BMC Cell Biol.*, 10, 16, **2009**
[11] S. V. Morozov, K. S. Novoselov, A. K. Geim, Electronic transport in graphene, *Physics – Uspekhi*, 178, 776, **2008**.
[12] D. C. Elias, R. V. Gorbachev, A. S. Mayorov, S. V. Morozov, A. A. Zhukov, P. Blake, L. A. Ponomarenko, I. V. Grigorieva, K. S. Novoselov, F. Guinea, A. K. Geim, Dirac cones reshaped by interaction effects in suspended graphene, *Nature Physics*, 8, 172, **2012**.
[13] H. V. Grushevskaya, G. G. Krylov, Charge carriers asymmetry and energy minigaps in monolayer graphene: Dirac – Hartree – Fock approach, *J. Nonlin. Phen.in Complex Sys.*, 16, 2, 189-208, **2013**.
[14] H. V. Grushevskaya, G. Krylov, Partially breaking pseudo-Dirac band symmetry in graphene, *J. Nonlin. Phen.in Complex Sys.*, 17, 1, 86-96, **2014**.
[15] V. Labunov, B. Shulitski, A. Prudnikava, Y. P. Shaman, A. S. Basaev, Composite nanostructure of vertically aligned carbon nanotube array and planar graphite layer obtained by the injection CVD method,

*Semiconductor Physics, Quantum Electronics & Optoelectronics*, 13, 2, 137-141, **2010**.
[16] H.V. Grushevskaya, V.V. Hrushevski, N.G. Krylova, T.A. Kulahava, I.V. Lipnevich, T.I. Orekhovskaya, G.N. Semenkova, B.G. Shulitsky, Cell functioning characterization using spontaneous polarization hysteresis in thin Langmuir-Blodgett films with modified multi-walled carbon nanotubes and rare-earth atoms,*J. Nonlin. Phen.in Complex Sys.*, 13, 4, 396-408, **2010**.
[17] A. S. Egorov, H. V. Krylova, I. V. Lipnevich, B. G. Shulitsky, L. V. Baran, S. V. Gusakova, M. I. Govorov, Structure of modified multi-walled carbon nanotube clusters on conducting organometallic Langmuir - Blodgett films, *J. Nonlin. Phen.in Complex Sys.*, 15, 2, 121-137, **2012**.
[18] V. V. Hrushevski, V. P. Egorova, V. I. Krot, H. V. Krylova, I. V. Lipnevich, T. I. Orekhovskaya, B. G. Shulitsky, E. N. Golubeva, The effects of CNT-enhanced micellarcompactification of oligonucleotide in Raman and dielectric spectroscopy, *10 International Conference "Medical-Social Ecology of Person: Status and Perspectives"*, Minsk, Belarus, April 6-7, **2012** (in Russian) .
[19] O. V. Choruzhaja, V. A. Kashpur, D. A. Pesina, V. Ja. Maleev, The change of hydration at formation of DNA complexes with some intarcalators, *Biophys. Herald*, 24, 1, 5, **2010**(in Russian) .
[20] V. E. Obukhov, I. I. Abramov, H.V. Krylova, I.V. Lipnevich, T.I. Orekhovskaya, M. A. Belov, E.N. Golubeva, A. D. Shirjaeva, The spectroscopy of dielectric structures on alumina for impedance nanoelectronics, *VII International Scientific and Technical Conference "The Modern Methods of Materials Construction and Processing*, Minsk, Belarus, September 19-21, **2012** (in Russian) .
[21] H. V. Grushevskaya, I. V. Lipnevich, T. I. Orekhovskaya, Coordination interaction between rare earth and/or transition metal centers and thiophene series oligomer derivatives in ultrathin Langmuir-Blodgett films, *J. Mod. Phys*., 4, 7-17, **2013**.
[22] E. K. Aparcin, D.S. Novopashina, Y. V. Nastaushev, A.G. Ven'jaminova, The fluorescent-labeld single-wall carbon nanotubes and their hybrids with oligonucleotides, *Russian Nanotechnologies*, 7, 3, 38-45, **2012** (in Russian) .
[23] A.A. Veligura, A.S. Egorov, V.P. Egorova, H.V. Krylova, I.V. Lipnevich, B.G. Shulitsky, Fluorofor quenching in oligonucleotide layers self-organized on carbon nanotubes, *Uzhhorod University Scientific Herald. Series Physics.*, 34, 207-210, **2013** (in Russian) .
[24] M. V. Karachevtsev, O. S. Lytvyn, S. G. Stepanian, V. S. Leontiev, L. Adamowicz, V. A. Karachevtsev, SWNT-DNA and SWNT-polyC hybrids: AFM study and computer modeling*, J. Nanoscience and Nanotechnology*, 8, 3, 1473-1480, **2008**.
[25] D. R. Cooper, B. D'Anjou, N. Ghattamaneni, B. Harack, M. Hilke, A. Horth, N. Majlis, M. Massicotte, L. Vandsburger, E. Whiteway, V. Yu, Experimental Review of Graphene, *ISRN Condensed Matter Physic*s., 2012, 56, **2012**.
[26] C. Fantini, A. Jorio, M. Souza, M. S. Strano, M. S. Dresselhaus, M. A. Pimenta, Optical transition energies for carbon nanotubes from resonant Raman spectroscopy: environment and temperature effects, *Phys. Rev. Lett.*, 93, 147406, **2004**.
[27] A. G. Souza Filho, S. G. Chou, G. SamsonidzeGe, G. Dresselhaus, M. S. Dresselhaus, L. An, J. Liu, A. K. Swan, M. S. Ünlü, B. B. Goldberg, Stokes and anti-stokes Raman spectra of small-diameter isolated carbon nanotubes, *Phys. Rev. B*, 69, 115428, **2004**.
[28] A. V. Prieszhev, V. V. Tuchin, L. P. Shubochkin, *Laser diagnostics in biology and medicine*, Nauka, **1989**.
[29] H. Krylova, L. Hurski, *Spin polarization in strong correlated nanosystems,* LAP LAMBERT Academic Publishing, **2013**.
[30] L. V. Keldysh, Coulomb interaction in thin semiconductor and semimetal films,*Pis'maZh. Eksp. Teor.Fiz.*, 29, 11, 716-719, **1979**.

## 6. ACKNOWLEDGEMENTS

This study was supported by grants from the Ministry of Education and National Academy of Science, Republic of Belarus.